

Bulletin of Pioneering Researches of Medical and Clinical Science

Available online: https://bprmcs.com 2021 | Volume 1 | Issue 1 | Page: 57-68

Detection of Extracellular Vesicle Surface Proteins and microRNAs in Clustered Vesicles by Flow Cytometry Using a Single Step in Situ Approach

Kim Se-En1*, Mi Jeong Kim1

Abstract

Given the heterogeneous nature of cancers, accurate and specific diagnosis necessitates multiplexed biomarker detection. Extracellular vesicles (EVs) have emerged as promising candidates for liquid biopsy biomarkers in cancer due to their molecular cargo. Nevertheless, their nanoscale size poses significant technical challenges, highlighting the need for an efficient and straightforward detection strategy. In this study, we established a single step in situ detection approach capable of simultaneously identifying both surface proteins and internal miRNAs of EVs through flow cytometry. To achieve multiplexed detection in normal and cancer-derived EVs, we employed a CD63 antibody alongside molecular beacon-21. Moreover, a phospholipid-polymer-phospholipid conjugate was utilized to promote EV clustering, as confirmed by nanoparticle tracking analysis, thereby amplifying the detection signal. This method successfully enabled the differentiation of cancer-derived EVs using a flow cytometer. Overall, our findings demonstrate that single step in situ detection of multiple EV biomarkers via flow cytometry represents a rapid, simple, and minimally invasive liquid biopsy technique with potential applications in cancer and other disease diagnostics.

Keywords: Flow cytometer, Single step in situ detection, Extracellular Molecular beacon, Extracellular vesicle cluster

Corresponding author: Sabin Shrestha E-mail: Seunkim4980@gmail.com

How to Cite This Article: Se-En K, Kim MJ. Detection of Extracellular Vesicle Surface Proteins and microRNAs in Clustered Vesicles by Flow Cytometry Using a Single Step In Situ Approach. Bull Pioneer Res Med Clin Sci. 2021;1(1):57-68. https://doi.org/10.51847/uzNTCM0gZ0

Introduction

In recent years, extracellular vesicles (EVs) have gained considerable attention as promising sources of innovative biomarkers for liquid biopsy, offering solutions to the associated with conventional biomarkers [1-3]. Functioning as essential mediators of intercellular communication, EVs—including exosomes—play significant roles in various biological particularly in cancer development, progression, and metastasis [4-8]. Elevated levels of EVs are present in a wide range of biological fluids such as blood [9], urine [10], saliva [11], and breast milk [12]. Due to their endosomal origin, EVs contain a rich diversity of biomolecules, including proteins and RNAs, which can either be encapsulated within their lumen or displayed on their surface [13, 14]. Among these, surface proteins and intravesicular microRNAs (miRNAs) have emerged as key targets for developing next-generation liquid biopsy biomarkers [15, 16]. Given the inherent heterogeneity of cancer, a single biomarker is often insufficient to accurately represent disease progression; therefore,

¹ Department of Bioengineering and Nano-Bioengineering, Incheon National University, Incheon 22012, Korea.

multiplexed detection is essential for achieving precise and reliable cancer diagnostics.

Current multiplex detection strategies for EV-associated proteins and miRNAs typically analyze each biomolecule separately using independent techniques such as real-time polymerase chain reaction (PCR) [17, 18] or enzymelinked immunosorbent assay (ELISA) [19]. Although these approaches are effective, they are time-consuming, costly, and labor-intensive, emphasizing the need for a streamlined and efficient method capable of detecting multiple EV biomarkers in a single step. Previously, we introduced a platform for the simultaneous multiplexed detection of EV surface proteins and internal miRNAs [20]. In that technique, EVs were initially captured with antibody-conjugated magnetic beads, followed by miRNA detection using molecular beacons (MBs) and nanoscale oligonucleotide probes [20-23], while surface proteins such as CD63 were labeled with fluorescently tagged antibodies. The resulting fluorescence intensities of both miRNAs and surface proteins were quantified using a fluorometer. Although this method offered a convenient and non-invasive diagnostic platform, it still required multiple washing steps, making the procedure relatively laborious.

To overcome these challenges, we developed a flow cytometry-based technique for single step in situ detection of both EV surface proteins and internal miRNAs (Figure 1A). Unlike conventional approaches, this method eliminates the need for washing steps and enables direct fluorescence measurement from individual EV particles via flow cytometry (Figure 1B). Furthermore, to enhance the detection sensitivity using a standard flow cytometer, we devised a strategy to induce EV clustering with a 1,2distearoyl-sn-glycero-3-phosphoethanolamine (DSPE)polyethylene glycol (PEG)-DSPE conjugate, which significantly amplified biomarker detection signals. This integrated approach not only simplifies the detection process but also improves the efficiency, accuracy, and cost-effectiveness of the assay. Given the heterogeneous nature of cancers and the clinical need for high-throughput diagnostic systems, this method offers a promising and practical platform for prognostic assessment and monitoring therapeutic responses in cancer patients.

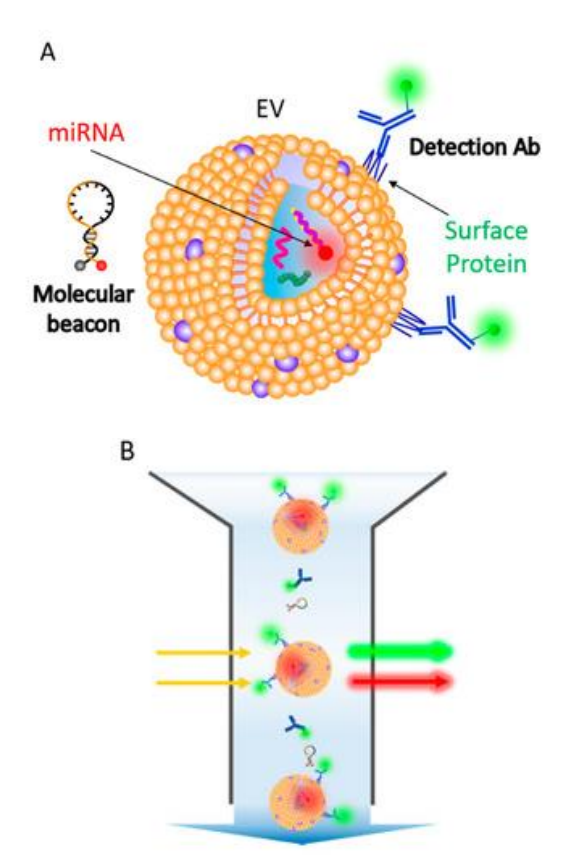


Figure 1. Illustration of the single step in situ detection strategy for extracellular vesicle (EV) surface proteins and miRNAs using flow cytometry. (A) Both EV surface markers and miRNA molecules are simultaneously visualized through fluorescently tagged antibodies and molecular beacons. (B) Flow cytometric one-step analysis enables concurrent detection of EV proteins and miRNAs

Materials and Methods

Cell culture and EV isolation

Human dermal fibroblasts (HDFs) were generously provided by Prof. K. M. Park (Incheon National University, Republic of Korea), while HeLa cells were obtained from the Korean Collection for Type Cultures. Both cell types—HDFs representing normal cells and HeLa representing cancer cells—were cultured in Dulbecco's Modified Eagle Medium (DMEM; Corning, NY, USA) supplemented with 10 percent fetal bovine serum (FBS; Gibco, MD, USA) and 1 percent penicillin–streptomycin. Cells were maintained at 37 degrees Celsius in a humidified atmosphere containing 5% CO₂.

For EV collection, cultures were maintained in media containing EV-depleted FBS, which was produced by ultracentrifuging FBS at $120,000\times$ g for ten hours at 4 °C using a TLA-100.3 rotor (Optima TL-100; Beckman Coulter, USA). The supernatant was subsequently filtered through a 0.22 μ m cellulose acetate filter (GVS, Italy) and frozen at -80 degrees Celsius until use.

EVs were extracted using the ExoQuick-TCTM precipitation reagent (System Biosciences, USA) following the manufacturer's protocol. After culturing, cell-conditioned media were centrifuged at 3000× g for fifteen minutes at 4 °C to remove debris, filtered (0.22 μm), and incubated with ExoQuick-TCTM at 4 degrees Celsius overnight. The mixture was then centrifuged at 1500× g for 30 minutes at 4 degrees Celsius, and the resulting pellet was dissolved in 1× PBS and stored at −80 degrees Celsius for subsequent analyses.

Characterization of EVs and measurement of protein concentration

The concentration and particle size distribution of EVs were evaluated using nanoparticle tracking analysis (NTA) with the NanoSight NS300 system (Malvern Panalytical, UK). Analysis parameters included a threshold setting of 4, 30-second capture duration, and fewer than 100 particles per frame. The camera was manually focused to achieve optimal particle visibility. To determine total protein levels, the bicinchoninic acid (BCA) assay (Thermo Fisher Scientific, USA) was employed. Working reagents were prepared as recommended by the manufacturer, and both EV samples and protein standards were incubated with the reagent for 30 minutes at 37 °C. The absorbance was then measured at 562 nm using a spectrophotometer to calculate protein concentrations.

Extraction of exosomal RNA, cDNA synthesis, and real-time PCR

Exosomal RNA was isolated using the FavorPrepTM Tri-RNA Reagent (Favorgen Biotech, Taiwan) according to the supplier's instructions. RNA quality and concentration were assessed with a NanoDropTM Lite spectrophotometer (Thermo Fisher Scientific, USA).

For reverse transcription, miRNAs were converted to cDNA using the miScript RT II Kit (Qiagen, Germany) employing a stem-loop primer design. The resulting cDNA was subjected to quantitative real-time PCR (qPCR) using a StepOnePlus™ Real-Time PCR System (Thermo Fisher Scientific, USA) and the miScript SYBR® Green PCR Kit (Qiagen, Germany) specific for mature miRNA sequences.

Expression levels of miRNAs were normalized using U6 small nuclear RNA (snRNA) as an internal control, enabling reliable comparison of miRNA abundance in EV samples.

Dynamic light scattering and western blotting

The surface charge of extracellular vesicles (EVs) was assessed by dynamic light scattering (DLS) using a Malvern Zetasizer Nano ZS (Malvern Panalytical, UK) at twenty-five degrees Celsius. To maintain consistency, identical EV concentrations were used across samples,

with a laser intensity of four milliwatts and a wavelength of 633 nanometers.

For Western blot analysis, EVs were lysed in RIPA buffer (Rockland Immunochemicals, Pottstown, PA, USA). Protein concentrations were measured using the BCA assay, and samples were separated via SDS-PAGE: TSG101 under reducing conditions, and CD63 and CD81 under non-reducing conditions. Twenty micrograms of protein per sample were loaded for each comparison.

Blots were probed with primary antibodies: mouse anti-TSG101 (1:1000, Abcam, ab83, UK), mouse anti-CD63 (1:1000, MBL, MEX002-3, USA), mouse anti-CD81 (1:1000, Abcam, ab79559, UK), rabbit anti-Syntenin (1:2000, Abcam, ab133267, UK), rabbit anti-Hsc70 (1:500, Abcam, ab51052, UK), rabbit anti-GM130 (1:1000, Abcam, ab52649, UK), and rabbit anti-calnexin (1:1000, Cell Signaling, 2679S, USA). Detection employed HRP-conjugated secondary antibodies: antimouse (1:2000, Abcam, ab6728, UK) and anti-rabbit (1:1000, Cell Signaling, 7074S, USA), visualized with an enhanced chemiluminescence system (Bio-Rad, USA). Images were captured using the ChemiDoc™ XRS+ imaging platform (Bio-Rad, USA).

miRNA detection with molecular beacons

A molecular beacon (MB-21) targeting mature miR-21 was synthesized with the sequence: 5'-Cy5-GCGCGTCAACATCAGTCTGATAAGCTACGCGC-BHQ2-3' [20–23]. The Cy5-labeled MB was designed using UNAFold (IDT, Coralville, IA, USA) and manufactured by Integrated DNA Technologies.

To confirm specificity, MB-21 was incubated with either synthetic miR-21 or EV-derived miR-21 at thirty-seven degrees Celsius for one hour, and hybridization was monitored using a Varioskan[™] Flash Multimode Reader (Thermo Fisher Scientific, USA) at 650 nm excitation and 670 nm emission.

Flow cytometric analysis of EV CD63 and miR-21, and EV clustering

For flow cytometry-based detection, EVs from normal and cancer cells were incubated with Alexa Fluor® 488-conjugated anti-CD63 antibody (1:50 volume ratio, Thermo Fisher Scientific, USA) for surface protein labeling, along with 100 nM MB-21 for miRNA detection, at thirty-seven degrees Celsius for one hour. Fluorescence signals were acquired either in a 384-well plate using a VarioskanTM Flash Multimode Reader or via a CytoFLEX flow cytometer (Beckman Coulter, USA). Quality control was performed biweekly using CytoFLEX Daily QC Fluorospheres.

During flow cytometric acquisition, the sample flow rate was set to ten microliters per minute, with data collection stopping after three hundred seconds or ten thousand events, whichever occurred first. Data analysis was performed in CytExpert (Beckman Coulter, USA). Fluorescence detection used 495 nm excitation/519 nm emission for CD63 and 650 nm excitation/670 nm emission for MB-21.

To enhance detection, EVs were induced to form clusters by incubating with DSPE-PEG-DSPE (0.5 mg/mL), 100 nM MB-21, and antibody (1:50 volume ratio) with 1×10^{10} EVs at thirty-seven degrees Celsius for two hours. PEG with a molecular weight of 10 kilodaltons was included in the reaction. Fluorescence signals were then analyzed using a fluorometer or flow cytometer.

Statistical analysis

Differences between two groups were assessed using a paired t-test in GraphPad Prism 7 (GraphPad Software, San Diego, CA, USA).

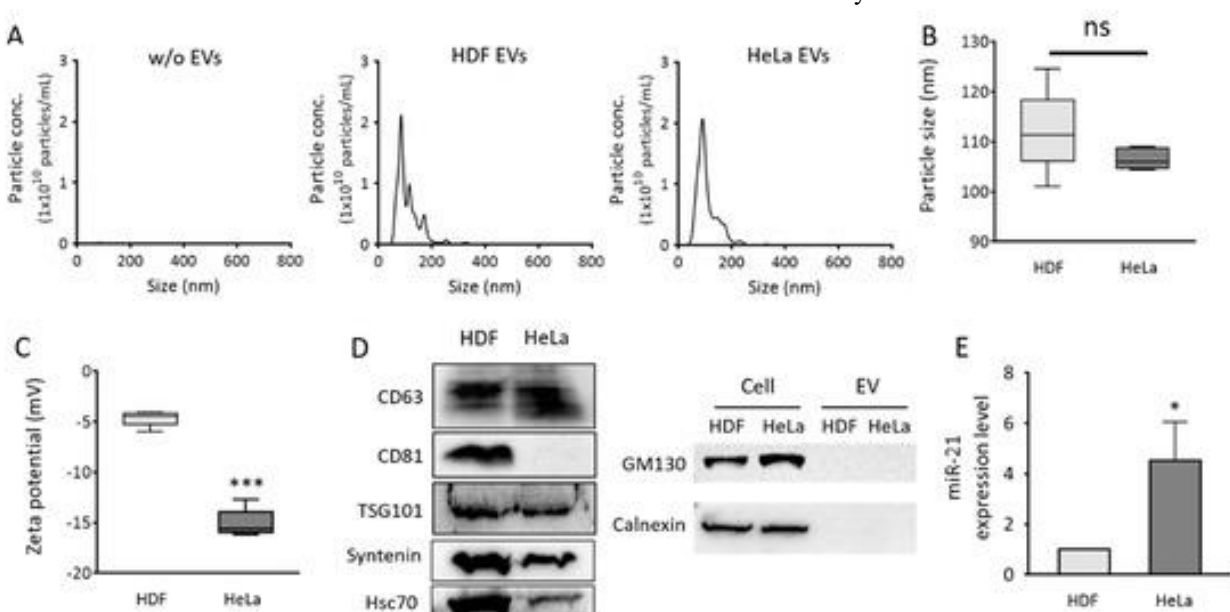


Figure 2. Characterization of EVs from normal and cancer cells: size, zeta potential, protein markers, and miR-21 content. Extracellular vesicles (EVs) were collected from normal human dermal fibroblasts (HDF) and cancerous HeLa cells using the ExoQuick-TCTM precipitation method. (A) Particle size distributions of HDF (middle) and HeLa (right) EVs were determined by nanoparticle tracking analysis (NTA), with PBS serving as a blank control. (B) Average particle diameters. (C) Zeta potentials for EVs derived from both cell types. (D) Western blotting was conducted to detect EV-associated proteins (CD63, CD81, TSG101, Syntenin, Hsc70) and non-EV contaminants (GM130, calnexin), with 20 μ g of EV protein loaded per lane. (E) Quantitative real-time PCR measured miR-21 levels in EVs, normalized to U6 snRNA. Data are shown as mean \pm SD (* p < 0.05, *** p < 0.001; ns: not significant; n = 3)

Western blot results confirmed the successful enrichment of EVs, as indicated by strong signals for CD63, CD81, TSG101, Syntenin, and Hsc70, while GM130 and calnexin were minimally detected (Figure 2D). Among the EVs, HeLa-derived particles exhibited lower CD81 but slightly higher CD63 compared with HDF EVs, leading to the selection of CD63 as the representative surface marker for subsequent flow cytometric analysis. Analysis of miR-21 by real-time PCR revealed that EVs from cancer cells contained approximately 4.5 times more miR-21 than those from normal cells (Figure 2E), aligning with

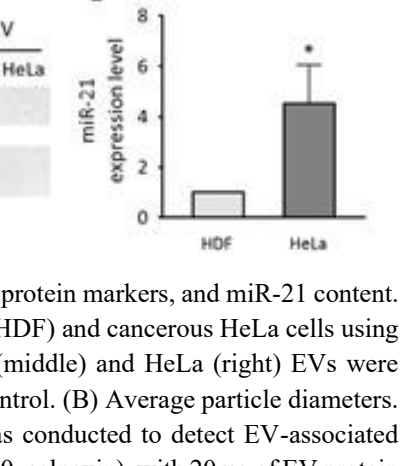
Characterization of normal and cancer-derived EVs To establish the single step in situ detection approach, EVs

Results

from HDFs (normal) and HeLa cells (cancer) were first characterized. Nanoparticle tracking analysis (NTA) revealed particle size distributions and concentrations (**Figure 2A**), with mean diameters of 112 nm for HDF EVs and 106 nm for HeLa EVs (**Figure 2B**).

The zeta potentials were measured as -4.68 mV for normal EVs and -15.08 mV for cancer EVs (Figure 2C), confirming a slightly negative surface charge for both populations. These findings are consistent with previous reports indicating that cancer-derived EVs carry a more negative charge than normal EVs [24]. Since ExoQuick-TC was used without additional purification, NTA

measurements may include minor contaminants.



previous reports [25, 26] and supporting its role as a potential cancer biomarker. Consequently, miR-21 was chosen as the EV miRNA marker for flow cytometry detection.

Direct detection of EV miR-21 using molecular beacons (MB)

The miR-21-specific molecular beacon (MB-21) was initially evaluated in solution to confirm its hybridization response at various target concentrations. Fluorescence intensity increased progressively and proportionally with

miR-21 concentration, showing a 13.4-fold rise when the target increased from 0 to 100 nM (Figure 3A). Encouraged by this, MB-21 was applied to EVs for direct, in situ detection (Figure 3B). EVs ranging from 0 to 20×10^7 particles/ μ L were incubated with MB-21, and fluorescence signals were recorded. Negligible signal was observed in the absence of EVs, while fluorescence grew substantially as EV concentration increased. These results demonstrate that MB-21 enables effective in situ detection of miR-21 within EVs.

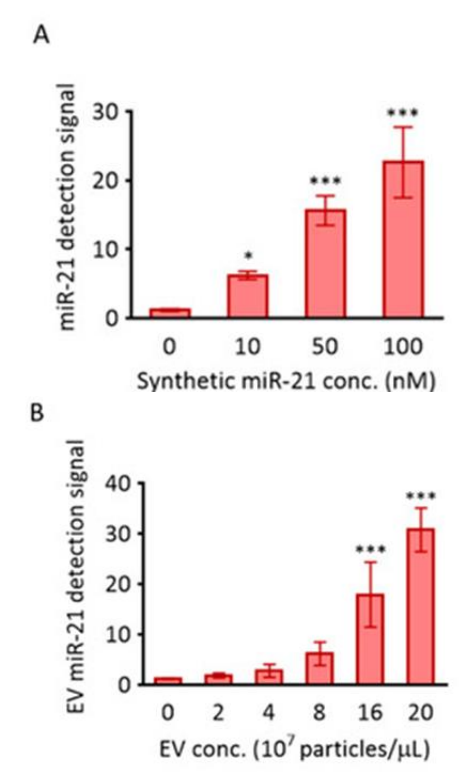


Figure 3. miR-21 detection using MB-21. The molecular beacon MB-21, specifically designed for miR-21, was assessed for hybridization both in solution (A) and in EVs derived from cancer cells (B). (A) MB-21 (100 nM) was incubated with varying concentrations of synthetic miR-21 (0–100 nM), and fluorescence signals were measured using a fluorometer. (B) MB-21 (100 nM) was incubated with different concentrations of HeLa cell-derived EVs (0–20 × 10⁷ particles/ μ L). Data are presented as mean \pm SD (* p < 0.05, *** p < 0.001; n = 3–6)

Non-EV-associated miRNAs can potentially interfere with detection, typically requiring protease/RNase treatment to remove miRNA-protein complexes. However, in situ detection with MB circumvents this step because proteins bound to miRNAs sterically hinder MB hybridization. Previous experiments comparing MB signals between untreated and RNase-treated EVs [23] showed no significant differences, confirming that pretreatment is unnecessary for MB-based in situ detection.

Fluorometric detection of EV miRNA and surface proteins

Due to their nanoscale size, EVs cannot be efficiently isolated or washed with standard centrifugation. Ultracentrifugation often results in significant EV loss, limiting its diagnostic utility. Polymer-based precipitation methods can co-precipitate contaminants such as proteins, highlighting the need for methods that allow direct, in situ detection of EV biomarkers for high-throughput liquid biopsy point-of-care applications. Achieving simultaneous detection of multiple EV biomarkers is critical for precise and specific diagnostics. The goal of the current method is to enable high-throughput disease detection through in situ EV biomarker profiling using flow cytometry. A key advantage of concurrently detecting EV surface proteins and miRNAs is the ability to differentiate EVs from potential contaminants, which rarely possess both markers simultaneously, and whose smaller size typically makes them undetectable by flow cytometry.

To test simultaneous in situ detection, MB-21 and fluorescently labeled antibodies against CD63 were incubated with or without EVs (2×10^8 particles/ μ L), and fluorescence signals were measured using a fluorometer. As shown in Figure 4A, high fluorescent signals were observed even in the absence of EVs, indicating that free, unbound CD63 antibodies contributed to the background signal due to the absence of a quencher. In contrast, MB-21 displayed minimal fluorescence without EVs, reflecting its self-quenching design (Figure 4B). Upon incubation with HDF-derived EVs, MB-21 fluorescence increased 2.4-fold, consistent with the presence of miR-21 detected by real-time PCR (Figure 2E). When incubated with HeLa EVs, fluorescence intensity rose 34-fold, aligning with the higher miR-21 content in cancer EVs. These findings highlight that unbound protein-targeting antibodies can significantly interfere with EV surface marker detection. Previous strategies for simultaneous miRNA and protein detection involved capturing EVs on magnetic beads and washing away unbound probes; however, this added step was necessary to separate true signals from background noise. The approach described here eliminates the need for washing, providing a simpler and more efficient method for in situ EV biomarker detection.

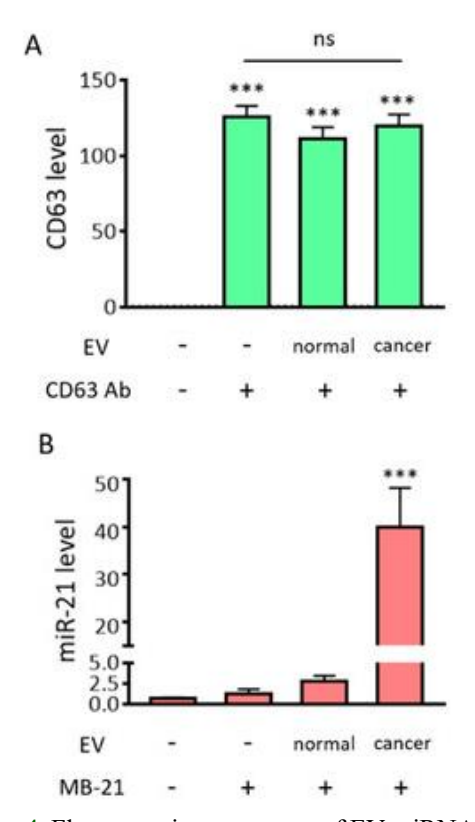


Figure 4. Fluorometric assessment of EV miRNAs and surface proteins. The ability to simultaneously detect EV surface protein (CD63) and miRNA (miR-21) in situ was evaluated using a fluorometer. (A) Fluorescence intensities of CD63-targeting antibodies were measured in the presence and absence of EVs. A substantial fluorescent signal was observed regardless of EV presence or type, indicating that unbound CD63 antibodies contribute to background signals and must be removed for specific EV detection. (B) Fluorescence from MB-21 was also measured with or without EVs. Minimal signal was detected in the absence of EVs due MB's self-quenching property. Fluorescence increased when MB-21 was incubated with normal EVs and showed a further rise with cancer-derived EVs. Data are expressed as mean \pm SD (*** p < 0.001; ns: not significant; n = 3-4)

Single-Step in situ flow cytometric detection of EV surface protein and miRNA

Previously, we developed a multiplexed in situ detection strategy for EV biomarkers using magnetic beads [20], where fluorescent signals of miRNAs and surface proteins were measured in solution with a fluorometer. This method required removal of unbound EVs through washing steps. Unlike MBs, which have intrinsic selfquenching due to a quencher, free antibodies produce fluorescence even when unbound, necessitating additional washing steps to eliminate background signals. These steps are labor-intensive and can lead to EV loss, potentially reducing detectable signals. Moreover, measuring average fluorescence from a subset of EVs may result in under- or overestimation of biomarker levels. Therefore, a method capable of distinguishing bound from unbound probes is essential for true single-step EV biomarker detection. Flow cytometry offers advantage, enabling analysis without removal of unbound probes, though traditional flow cytometers face challenges in detecting nanoscale particles such as EVs.

To assess this, EVs were labeled simultaneously with fluorescent antibodies and MBs for single-step in situ flow cytometric detection of surface protein and miRNA. Free CD63 antibodies and MB-21 in the absence of EVs were first confirmed to produce no detectable signal (Figure 5A). Next, normal EVs from HDF cells were analyzed without probes (Figure 5B) and in the presence of CD63 antibody and MB-21 (Figure 5C). Fluorescence increased for both CD63 and miR-21 when the probes were added, indicating successful detection of surface CD63 and internal miR-21. Specifically, the CD63-positive population increased from 2.0 percent to 17.7 percent, and the miR-21-positive population rose from 4.4 percent to 17.7 percent, as shown in quadrant plots. Although many particles in the main peak exhibited low fluorescence likely due to low CD63/miR-21 levels or EVs being below the detectable size threshold—a significant fraction of EVs were successfully recognized, demonstrating that antibody-labeled EVs can be detected without requiring any washing steps.

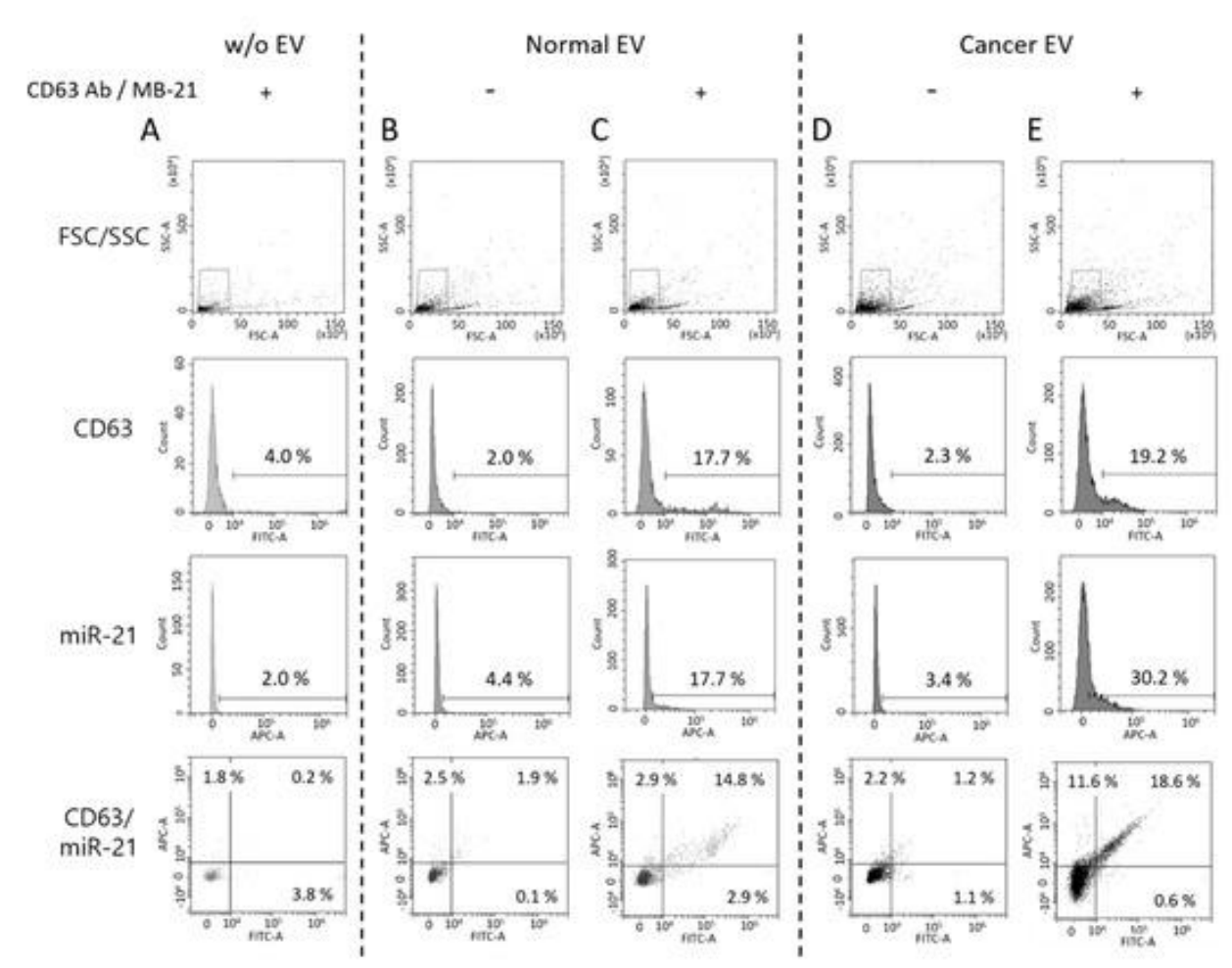


Figure 5. Single-step flow cytometric profiling of EV surface markers and miRNAs. Flow cytometry was applied to simultaneously monitor CD63 and miR-21 in EVs using a one-step approach. Forward and side scatter (FSC/SSC) gating is shown in the top panel. (A) Control experiments with CD63 antibody and MB-21 in the absence of EVs confirmed negligible background signal. (B, C) Normal EVs were analyzed without (B) and with (C) the addition of CD63 antibody and MB-21. Background fluorescence was measured from EVs lacking probes. Quadrant plots indicate the percentages of CD63-positive (x-axis) and miR-21-positive (y-axis) EVs, revealing clear signal enhancement in the presence of the detection probes. (D, E) HeLa-derived cancer EVs were similarly evaluated without (D) and with (E) probes. Compared to normal EVs, miR-21-positive EVs were more abundant in the cancer sample, leading to a larger fraction of EVs simultaneously positive for CD63 and miR-21

In a detailed analysis of cancer EVs from HeLa cells, flow cytometry showed minimal fluorescence in the absence of detection probes, with CD63-positive EVs at 2.3% and miR-21-positive EVs at 3.4% (Figure 5D). Following labeling with CD63 antibody and MB-21, the CD63-positive population rose to 19.2%, while miR-21-positive EVs increased to 30.2% (Figure 5E). The quadrant plots illustrate distinct molecular profiles: although the proportion of CD63-positive EVs was comparable between normal and cancer EVs, the fraction of miR-21-positive EVs was considerably higher in cancer EVs. These findings confirm that flow cytometry can achieve effective single-step detection of EV surface proteins and encapsulated miRNAs without the need for washing or separation steps.

Induction of EV clustering using DSPE-PEG-DSPE

Although single-step flow cytometry enabled detection of EV proteins and miRNAs, a fraction of EVs remained undetected, likely due to their nanoscale size. Conventional flow cytometers, optimized for cellular analysis, often struggle to detect such small particles. While high-resolution flow cytometry could improve EV detection, our goal was to enhance biomarker analysis using standard flow cytometers. Increasing the effective size of EVs could therefore improve both detection efficiency and accuracy in this context.

To address this, we developed a strategy to promote EV clustering using a phospholipid–polymer–phospholipid conjugate, DSPE-PEG-DSPE (Figure 6A). In this conjugate, DSPE serves as the lipid anchor, while PEG functions as a flexible linker [27-29]. The design principle is that one DSPE moiety can integrate into the membrane of a single EV, while the opposite DSPE can bind another

EV, allowing multiple EVs to be connected into clusters. This clustering is expected to increase the apparent particle size, facilitating detection by a standard flow cytometer. To test this approach, EVs were incubated with 0.5 mg/mL DSPE-PEG-DSPE for 2 hours, and particle sizes were measured before and after treatment using nanoparticle tracking analysis (NTA) (Figure 6B, C). Treatment with DSPE-PEG-DSPE resulted in the formation of clusters larger than individual EVs. The average particle size

increased from 100 nm to 110 nm, and the main peak shifted from 82 nm to 101 nm. These results suggested that clustering via DSPE-PEG-DSPE could potentially enhance simultaneous in situ detection of EV biomarkers. Given that NTA measurements can exhibit systematic fluctuations, further validation using transmission electron microscopy was needed to directly visualize EV clusters and estimate the number of EVs per cluster.

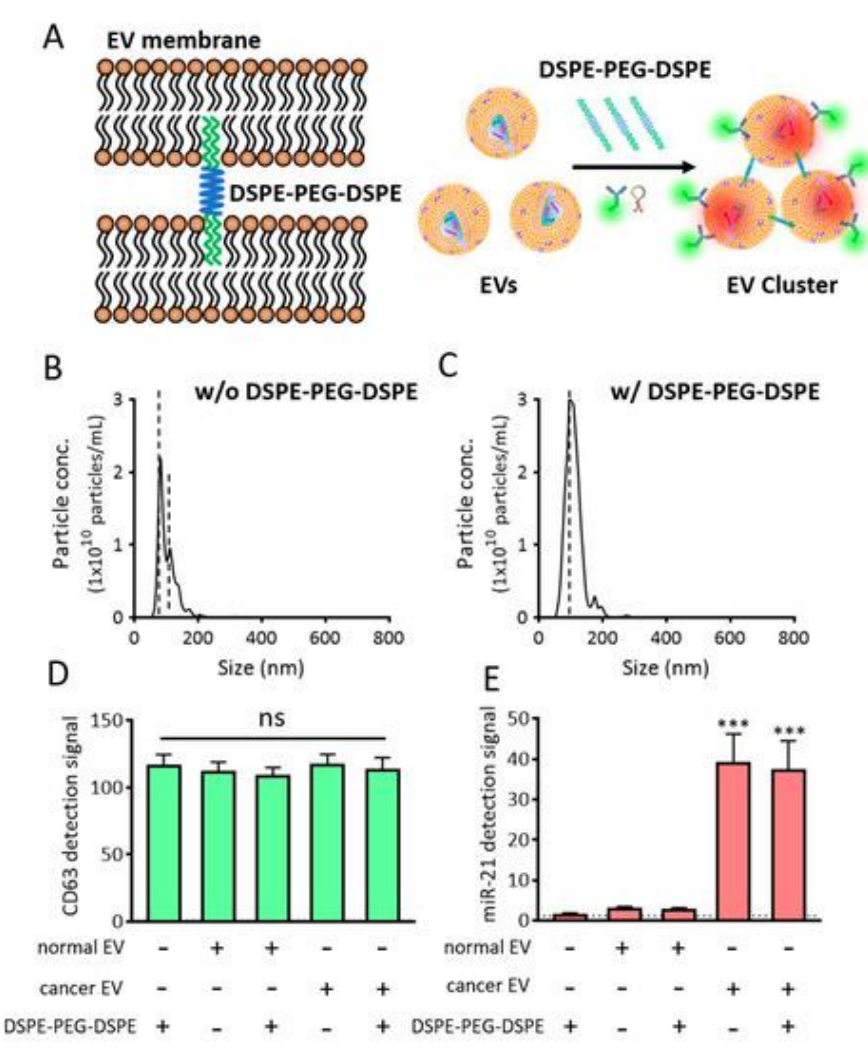


Figure 6. Formation of EV clusters via DSPE-PEG-DSPE. (A) Schematic illustrating how DSPE-PEG-DSPE promotes EV clustering and enables single-step detection of EV biomarkers using flow cytometry. (B, C) NTA analysis of cancer EVs showing particle size distributions in the absence (B) and presence (C) of DSPE-PEG-DSPE, with clustered EVs appearing larger than individual EVs. (D, E) Fluorescence measurements of CD63 (D) and miR-21 (E) in the presence of DSPE-PEG-DSPE, assessed using a fluorometer. Data are expressed as mean \pm SD (*** p < 0.001; ns: not significant; n = 3-6)

Before optimizing biomarker detection in clustered EVs, we evaluated whether DSPE-PEG-DSPE interferes with fluorescence signals. Incubation of DSPE-PEG-DSPE with CD63-targeting antibodies (Figure 6D) or MB-21 (Figure 6E) did not alter fluorescence intensities, indicating no interaction or clustering of the probes themselves. Furthermore, co-incubation of normal or cancer EVs with DSPE-PEG-DSPE and detection probes

showed no significant changes in fluorescence signals, confirming that DSPE-PEG-DSPE does not affect fluorometer-based measurements.

Single-Step in situ detection of EV proteins and miRNAs in clusters

To detect EV surface proteins and internal miRNAs simultaneously, EVs were incubated with DSPE-PEG-

DSPE for 2 hours in the presence of CD63 antibody and MB-21, followed by flow cytometric analysis. Given that DSPE-PEG-DSPE can self-assemble into micelles, we first assessed whether these structures influence detection by incubating DSPE-PEG-DSPE with CD63 antibody and MB-21 in the absence of EVs. As shown in **Figure 7A**, only 16.2 percent and 0.8 percent of events were positive for CD63 and miR-21, respectively, demonstrating that self-assembly did not interfere with flow cytometric detection.

Next, normal EVs were co-incubated with DSPE-PEG-DSPE, CD63 antibody, and MB-21 and analyzed (Figure 7B, C). The fraction of CD63-positive EVs increased from 20.4% to 32.3% after clustering, indicating enhanced

detection due to the formation of EV clusters. In contrast, miR-21-positive EVs did not show a comparable increase, likely reflecting the low intrinsic levels of miR-21 in EVs from normal cells. Additionally, variations in EV membrane stiffness from different cell types may influence clustering efficiency and warrant further investigation to understand how membrane properties affect DSPE-PEG-DSPE insertion and cluster formation. Quadrant gating was used to distinguish CD63-positive, miR-21-positive, and double-negative EVs. Overall, clustering normal EVs with DSPE-PEG-DSPE enabled simultaneous detection of both biomarkers in a single-step assay using CD63 antibody and MB-21.

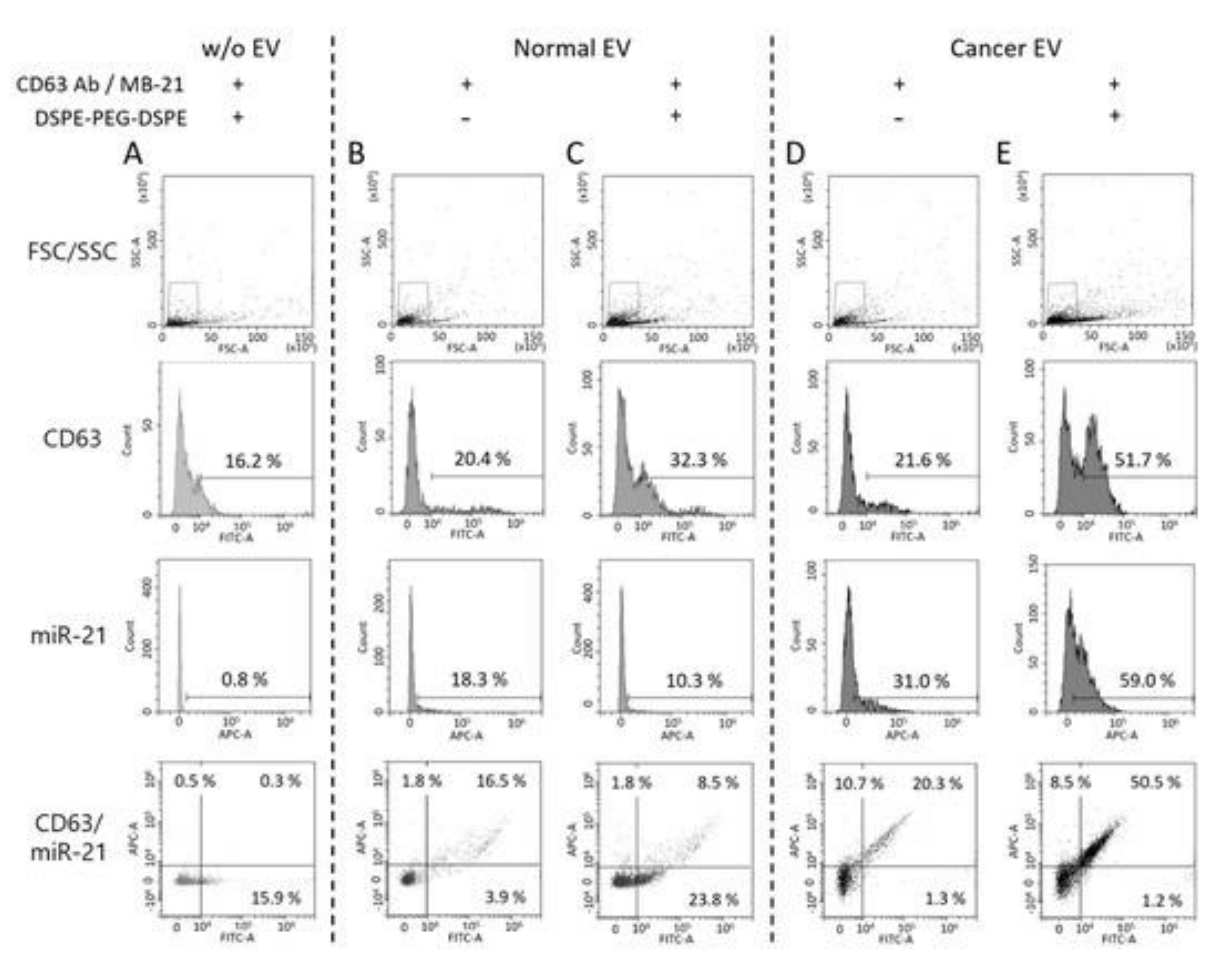


Figure 7. Single-step in situ detection of proteins and miRNAs in clustered EVs via flow cytometry. Forward and side scatter (FSC/SSC) gating is shown in the top panel. (A) DSPE-PEG-DSPE was incubated with CD63 antibody and MB-21 in the absence of EVs to assess background signals. (B, C) Normal EVs were analyzed without (B) or with (C) DSPE-PEG-DSPE in the presence of CD63 antibody and MB-21. Quadrant plots display percentages of CD63-positive (x-axis) and miR-21-positive (y-axis) EVs, allowing visualization of the populations carrying one or both biomarkers. (D, E) Cancer EVs were similarly assessed in the absence (D) or presence (E) of DSPE-PEG-DSPE. Clustering EVs with DSPE-PEG-DSPE enhanced the detection efficiency of both CD63 and miR-21, resulting in increased percentages of biomarker-positive EVs. Notably, cancer EVs exhibited a more pronounced rise in populations positive for both markers compared to normal EVs

To evaluate single-step biomarker detection in cancerderived EV clusters, HeLa cell EVs were incubated with CD63 antibody and MB-21, with or without DSPE-PEG- DSPE (Figure 7D, E). Without clustering, 21.6% of EVs were CD63-positive and 31.0% were miR-21-positive, already higher than normal EVs. Upon DSPE-PEG-DSPE-

induced clustering, these populations increased substantially to 51.7% for CD63 and 59.0% for miR-21, with 50.5% of EVs positive for both markers simultaneously, as shown in the quadrant plots. For comparison, the percentages of CD63 and miR-21 positive EVs were only 8.5% and 20.3% in clustered normal and unclustered cancer EVs, respectively. These findings indicate that clustering EVs using DSPE-PEG-DSPE significantly enhances the efficiency of single-step in situ detection of protein and miRNA biomarkers using flow cytometry.

The impact of DSPE-PEG-DSPE clustering is further illustrated in merged flow cytometry analyses of normal and cancer EVs (Figure 8A, B). Median fluorescence intensities for CD63 and miR-21 were significantly higher following cluster formation (Figure 8C, D). Importantly, the dramatic increase in biomarker-positive populations occurred despite only modest changes in particle size after clustering, suggesting that the effective size increase falls within the flow cytometer's detection threshold. Additional studies are needed to investigate the relationship between EV size and detection sensitivity in flow cytometry.

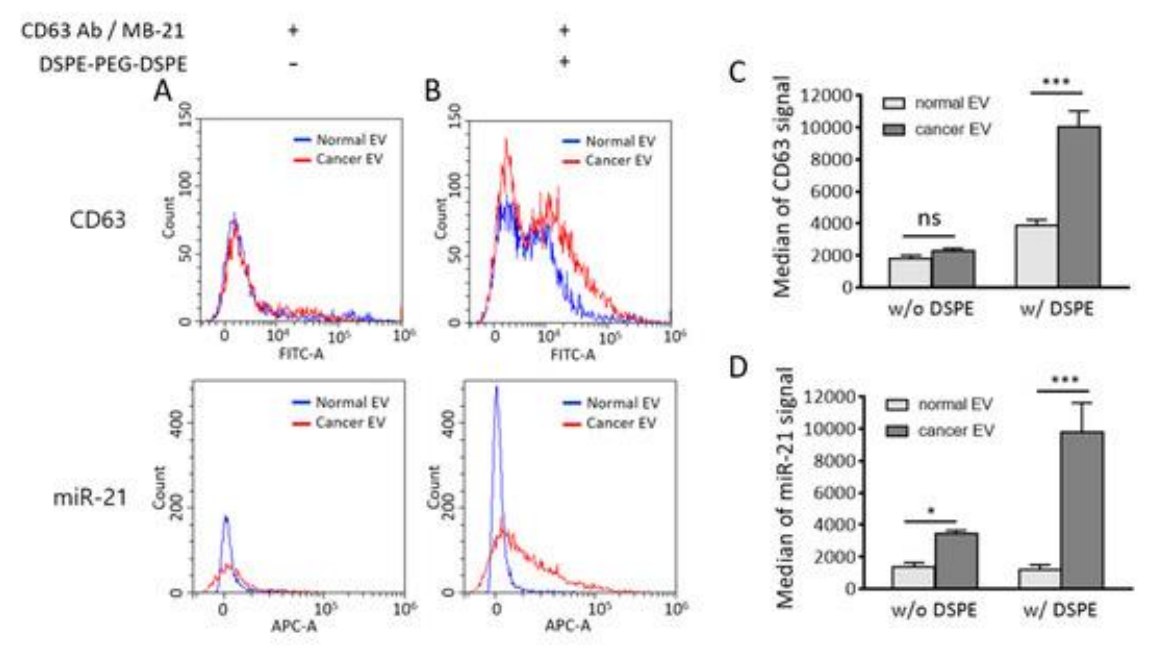


Figure 8. Flow cytometric comparison of normal and cancer EVs with and without DSPE-PEG-DSPE. (A, B) Overlayed flow cytometry data show CD63 (top) and miR-21 (bottom) signals for normal and cancer EVs in the absence (A) and presence (B) of DSPE-PEG-DSPE. (C, D) Median fluorescence intensities for CD63 (C) and miR-21 (D) were quantified from the flow cytometry results. Data are presented as mean \pm SD (* p < 0.05, *** p < 0.001; ns: not significant; n = 3)

It is possible that DSPE-PEG-DSPE could alter EV membrane properties, potentially allowing greater MB-21 uptake and enhancing detection of miR-21-positive cancer EVs. In theory, increased DSPE insertion might facilitate more MB-miRNA hybrid formation and stronger fluorescence signals. However, fluorometer measurements (**Figure 6E**) indicated that miR-21 levels detected by MB-21 were comparable between clustered and non-clustered cancer EVs, suggesting that the observed rise in miR-21-positive populations in flow cytometry was not due to changes in membrane permeability caused by DSPE-PEG-DSPE.

Previously, multiplexed EV biomarker detection using magnetic bead capture faced several limitations. The process was labor-intensive and time-consuming, making it unsuitable for high-throughput applications. Low capture efficiency resulted in substantial EV loss during sample preparation, and proximity between iron oxide beads and EVs could quench fluorescence, reducing signal

accuracy. Direct evidence for DSPE-PEG-DSPE-mediated EV cluster formation still requires further study, and optimization for clinical samples such as human serum or urine is needed. Overall, this bead-free, in situ flow cytometric approach overcomes these challenges, enabling simultaneous detection of EV proteins and miRNAs. To our knowledge, this is the first report demonstrating flow cytometric analysis of multiple EV biomarkers through induced EV clustering using DSPE-PEG-DSPE.

Conclusions

Extracellular vesicles (EVs) are challenging to manipulate due to their nanoscale size, making the development of efficient and straightforward methods for EV biomarker detection crucial. Furthermore, strategies enabling multiplexed detection of biomarkers within individual EVs are needed to enhance their utility compared to other

circulating biomarkers in liquid biopsy. In this study, we introduce a method for simultaneous, single-step, in situ detection of EV surface proteins and internal miRNAs using flow cytometry. To improve detection sensitivity, DSPE-PEG-DSPE was employed to induce EV clustering, which amplified the signals generated by the detection antibody and molecular beacon. This approach demonstrates that single-step, in situ detection of multiple EV biomarkers via flow cytometry can serve as a simple, rapid, and non-invasive liquid biopsy technique, offering a valuable platform for disease diagnosis (including cancer), prognosis prediction, and monitoring therapeutic responses in clinical settings.

Acknowledgments: None.

Conflict of interest: None.

Financial support: None.

Ethics statement: None.

References

- Vasconcelos MH, Caires HR, Ābols A, Xavier CP, Linē A. Extracellular vesicles as a novel source of biomarkers in liquid biopsies for monitoring cancer progression and drug resistance. Drug Resist Update. 2019;47:100647.
- 2. Marrugo-Ramirez J, Mir M, Samitier J. Blood-based cancer biomarkers in liquid biopsy: a promising non-invasive alternative to tissue biopsy. Int J Mol Sci. 2018;19:2877.
- 3. Minciacchi VR, Zijlstra A, Rubin MA, Di VD. Extracellular vesicles for liquid biopsy in prostate cancer: where are we and where are we headed? Prostate Cancer Prostatic Dis. 2017;20:251–8.
- 4. Azmi AS, Bao B, Sarkar FH. Exosomes in cancer development, metastasis, and drug resistance: a comprehensive review. Cancer Metastasis Rev. 2013;32:623–42.
- An T, Qin S, Xu Y, Tang Y, Huang Y, Situ B, et al. Exosomes serve as tumour markers for personalized diagnostics owing to their important role in cancer metastasis. J Extracell Vesicles. 2015;4:27522.
- Patil AA, Rhee WJ. Exosomes: biogenesis, composition, functions, and their role in premetastatic niche formation. Biotechnol Bioprocess Eng. 2019;24:689–701.
- 7. Kim H, Rhee WJ. Exosome-mediated Let7c-5p delivery for breast cancer therapeutic development. Biotechnol Bioprocess Eng. 2020;25:513–20.
- 8. Jeong K, Yu YJ, You JY, Rhee WJ, Kim JA. Exosome-mediated microRNA-497 delivery for anti-

- cancer therapy in a microfluidic 3D lung cancer model. Lab Chip. 2020;20:548–57.
- Caby MP, Lankar D, Vincendeau-Scherrer C, Raposo G, Bonnerot C. Exosomal-like vesicles are present in human blood plasma. Int Immunol. 2005;17:879–87.
- Cho S, Yang HC, Rhee WJ. Development and comparative analysis of human urine exosome isolation strategies. Process Biochem. 2020;88:197– 203.
- 11. Ogawa Y, Miura Y, Harazono A, Kanai-Azuma M, Akimoto Y, Kawakami H, et al. Proteomic analysis of two types of exosomes in human whole saliva. Biol Pharm Bull. 2011;34:13–23.
- Admyre C, Johansson SM, Qazi KR, Filén JJ, Lahesmaa R, Norman M, et al. Exosomes with immune modulatory features are present in human breast milk. J Immunol. 2007;179:1969–78.
- 13. Rabinowits G, Gerçel-Taylor C, Day JM, Taylor DD, Kloecker GH. Exosomal microRNA: a diagnostic marker for lung cancer. Clin Lung Cancer. 2009;10:42–6.
- Munson P, Shukla A. Exosomes: potential in cancer diagnosis and therapy. Medicines (Basel). 2015;2:310–27.
- Boriachek K, Islam N, Möller A, Salomon C, Nguyen N, Hossain SA, et al. Biological functions and current advances in isolation and detection strategies for exosome nanovesicles. Small. 2018;14:1702153.
- 16. Soung YH, Ford S, Zhang V, Chung J. Exosomes in cancer diagnostics. Cancers (Basel). 2017;9:8.
- 17. Nabet BY, Qiu Y, Shabason JE, Wu TJ, Yoon T, Kim BC, et al. Exosome RNA unshielding couples stromal activation to pattern recognition receptor signaling in cancer. Cell. 2017;170:352–66.
- Hannafon BN, Trigoso YD, Calloway CL, Zhao YD, Lum DH, Welm AL, et al. Plasma exosome microRNAs are indicative of breast cancer. Breast Cancer Res. 2016;18:90.
- Yokoyama S, Takeuchi A, Yamaguchi S, Mitani Y, Watanabe T, Matsuda K, et al. Clinical implications of carcinoembryonic antigen distribution in serum exosomal fraction—measurement by ELISA. PLoS One. 2017;12:e0183337.
- Cho S, Yang HC, Rhee WJ. Simultaneous multiplexed detection of exosomal microRNAs and surface proteins for prostate cancer diagnosis. Biosens Bioelectron. 2019;146:111749.
- 21. Lee JH, Kim JA, Kwon MH, Kang JY, Rhee WJ. In situ single step detection of exosome microRNA using molecular beacon. Biomaterials. 2015;54:116–25.

- 22. Lee JH, Kim JA, Jeong S, Rhee WJ. Simultaneous and multiplexed detection of exosome microRNAs using molecular beacons. Biosens Bioelectron. 2016;86:202–10.
- Lee J, Kwon MH, Kim JA, Rhee WJ. Detection of exosome miRNAs using molecular beacons for diagnosing prostate cancer. Artif Cells Nanomed Biotechnol. 2018;46(Suppl 3):S52–63.
- 24. Akagi T, Kato K, Hanamura N, Kobayashi M, Ichiki T. Evaluation of desialylation effect on zeta potential of extracellular vesicles secreted from human prostate cancer cells by on-chip microcapillary electrophoresis. Jpn J Appl Phys. 2014;53:06JL01.
- Yan LX, Huang XF, Shao Q, Huang MY, Deng L, Wu QL, et al. MicroRNA miR-21 overexpression in human breast cancer is associated with advanced clinical stage, lymph node metastasis and poor prognosis. RNA. 2008;14:2348–60.
- Si ML, Zhu S, Wu H, Lu Z, Wu F, Mo YY. miR-21-mediated tumor growth. Oncogene. 2007;26:2799–803.

- 27. Kim MS, Haney MJ, Zhao Y, Yuan D, Deygen I, Klyachko NL, et al. Engineering macrophage-derived exosomes for targeted paclitaxel delivery to pulmonary metastases: in vitro and in vivo evaluations. Nanomedicine. 2018;14:195–204.
- 28. Zhu Q, Ling X, Yang Y, Zhang J, Li Q, Niu X, et al. Embryonic stem cells-derived exosomes endowed with targeting properties as chemotherapeutics delivery vehicles for glioblastoma therapy. Adv Sci (Weinh). 2019;6:1801899.
- 29. Di H, Zeng E, Zhang P, Liu X, Zhang C, Yang J, et al. General approach to engineering extracellular vesicles for biomedical analysis. Anal Chem. 2019;91:12752–9.